Phys. Med. Biol. **54** (2009) 3421–3432 doi:10.1088/0031-9155/54/11/010

Dosimetry robustness with stochastic optimization

Omid Nohadani[1,2], **Joao Seco**[1], **Benjamin C Martin**[1] **and Thomas Bortfeld**[1]

[1] Department of Radiation Oncology, Massachusetts General Hospital and Harvard Medical School, Boston, MA 02114, USA
[2] Operations Research Center, Massachusetts Institute of Technology, Cambridge, MA 02139, USA

E-mail: nohadani@mit.edu, jseco@partners.org, ben.martin@alum.bu.edu and tbortfeld@partners.org

Received 27 December 2008, in final form 13 April 2009
Published 13 May 2009
Online at stacks.iop.org/PMB/54/3421

Abstract
All radiation therapy treatment planning relies on accurate dose calculation. Uncertainties in dosimetric prediction can significantly degrade an otherwise optimal plan. In this work, we introduce a robust optimization method which handles dosimetric errors and warrants for high-quality IMRT plans. Unlike other dose error estimations, we do not rely on the detailed knowledge about the sources of the uncertainty and use a generic error model based on random perturbation. This generality is sought in order to cope with a large variety of error sources. We demonstrate the method on a clinical case of lung cancer and show that our method provides plans that are more robust against dosimetric errors and are clinically acceptable. In fact, the robust plan exhibits a two-fold improved equivalent uniform dose compared to the non-robust but optimized plan. The achieved speedup will allow computationally extensive multi-criteria or beam-angle optimization approaches to warrant for dosimetrically relevant plans.

(Some figures in this article are in colour only in the electronic version)

1. Introduction

Intensity modulated radiation therapy (IMRT) has the ability to deliver highly conformal dose distributions to tumors of complex shapes. Uncertainties, however, can substantially degrade the quality of an otherwise optimized treatment plan. These uncertainties can have numerous sources, such as an imperfect setup during the treatment, imaging errors and organ motion. The issue of organ motion, particularly breathing motion, and setup errors during the treatment has been recently addressed using novel robust optimization techniques, e.g., by Chu *et al* (2005) and Chan *et al* (2006).

In all cases, computer simulations are employed in the process of treatment planning and dose calculation. However, the quality of these optimized plans significantly depends on how well the underlying dose calculation matches the actual dose delivered and any dosimetric discrepancy can degrade the treatment plan.

In this paper, we address the issue of dosimetric errors in the IMRT treatment planning. In particular, we present a method that takes these errors into account during optimization and provides a plan which is robust against possible dosimetric errors. These errors are estimated based on a quantitative comparison between different dose calculation techniques. To cover the spectrum of available techniques, we choose a pencil-beam (PB) based algorithm for the high-efficiency and low-accuracy end of this spectrum and a Monte Carlo (MC) based dose calculation for the low-efficiency but high-accuracy end. Since MC techniques are regarded as the 'gold standard' for accuracy, we use a PB dose calculation and model the deviations to the MC dose as dosimetric errors. We then introduce an optimization method which provides plans that are intrinsically robust against these errors and are comparable to MC-based plans. The main advantage of this method is that it uses high-efficiency PB dose calculations and provides high-accuracy plans, which constitute a significant speedup. Moreover, this method allows us to take into account other sources of errors, which affect the dosimetric aspects.

Currently, commercial software for IMRT optimization yield acceptable performance. In the recent past, there has been a sizable body of literature on accelerating IMRT optimization. Many available planning systems rely on approximative dose calculations which are then verified prior to treatment delivery (Intensity Modulated Radiation Therapy Collaborative Working Group 2001, Zakarian and Deasy 2004). Within the context of traditional planning techniques, faster optimization allows the treatment planner to take more attempts at finding the best plan. This is important because the appropriate parameters for the IMRT optimization are usually not clear until after some experimentation, and test runs are done for a given patient. Additionally, the importance attached to each constraint needs to be adapted in order to find the best trade-off between sparing normal tissue and tumor control, requiring more runs.

Multi-criteria optimization is an approach to help the treatment planner assess the various trade-offs in IMRT optimization. One approach is to pre-calculate and store a large number of plans with different parameters as described by Küfer *et al* (2003). The user can then explore the space of available plans very quickly. Faster optimization allows this database of plans to be computed faster and to include more plans (Craft and Bortfeld 2008). Beam angle optimization is another area where a large number of plans are necessary. In standard practice, a reasonable set of beam directions is preselected by the treatment planner. However, it would be preferable for the optimization to automatically find the best beam angles. This requires many runs for various sets of beam angles, so the computational speed is critical to making beam angle optimization practical.

In this work, we provide a method that allows the use of computationally less extensive PB dose calculation during the optimization while providing plans that are comparable to high-accuracy MC-based plans. This method relies on a generic model for dosimetric errors; thus, it can encompass imaging and numerical errors as well. To showcase the performance of this method, we apply it to an actual lung cancer patient and compare plans using different optimization techniques.

In section 2, we discuss how the data were collected from the lung cancer patient. In section 3, we introduce the two algorithms used to generate dose influence matrices, the PB and the MC algorithms. We introduce a clinically relevant MC-based IMRT optimized plan, which is the first of its kind to the best of our knowledge, in section 3. We then compare the same plan with a PB-based plan to showcase the discrepancies. The dosimetric errors are

estimated in section 5. In section 6, we introduce a robust optimization method that takes these errors into account during optimization; thus, it provides a plan that is inherently robust against dosimetric errors. The performance of this method is illustrated in section 7 by a quantitative comparison between resulting plans.

2. Data acquisition

For this study, we consider one lung cancer patient with a tumor target volume in order to cover a large subset of possible tumor scenarios. The patient had two sets of pre-treatment CT scans taken using helical CT: (a) a 'free-breathing' scan and (b) an axial cine-mode scan. All 4D CT data were acquired on a GE lightspeed Qx/I four-slice CT scanner. For thorax scan, a current of 170 mA was used for the 140 kV tube potential with a CT slice thickness of 2.5 mm, helical pitch of 7.5 mm per rotation and gantry rotation speed of 0.8 s per rotation. The total 3D helical scan took approximately 20 s.

The internal target volume (ITV) contouring was conducted by visual inspection of the tumor motion on all phases and then contouring a region of the free-breathing CT that encompasses all tumor motion. A margin was added to generate the planning target volume (PTV) in order to account for setup errors. Here, we address dosimetric errors; thus, we will consider the PTV only. The prescribed dose was 63 Gy for the PTV.

3. Dose calculation

To evaluate the dosimetric errors in the treatment planning, we compare dose calculation using the pencil beam algorithm, as implemented in CERR (Deasy *et al* 2003), and Monte Carlo dose calculation, as implemented in 4D MC, developed by Seco *et al* (2008) using the dose planning method (DPM), with ECUT and PCUT being 700 and 50 keV, respectively for a 6 MeV beam (Sempau *et al* 2000). This efficient and accurate code accounts for beam hardening and tongue-and-groove effect by using first Compton scatter in the MLC medium. The method was extended to allow photon transport through the JAWS and MLC using multiple Compton scatter. To incorporate temporal changes in the leaf position relative to the moving tumor target, different incidences in time were combined based on the prescribed monitor units, in order to reduce small MU effects (Seco *et al* 2007).

Of the first studies using MC for IMRT optimization, Jeraj and Keall (1999) performed optimization on MC-generated PB. In Jeraj and Keall (1999), an initial back-projection estimate was performed with MCNP to generate an initial IMRT fluence estimate. EGS4 was then used to generate the required PB for optimization of all beams. However, MLC delivery constraints, head scatter variations with field sizes and motion effects in the patient breathing or MLC delivery were not taken into account. More recently, Siebers *et al* (2007) proposed a hybrid method in which the initial dose prediction was preformed using a PB algorithm. For subsequent iterations, the PB dose prediction was improved by using the MC algorithm such that the optimized plans were equivalent to a full MC-based optimization but required a factor of $\sim$2.5 fewer MC dose computations. In this work, we employed MC to generate the pencil beam dose distributions for all the beamlets used in the optimization procedure and for five breathing phases (from inhale to exhale). Therefore, these MC-generated pencil beams account correctly for not only heterogeneity effects in the lung region, but also motion effects due to the patient breathing.

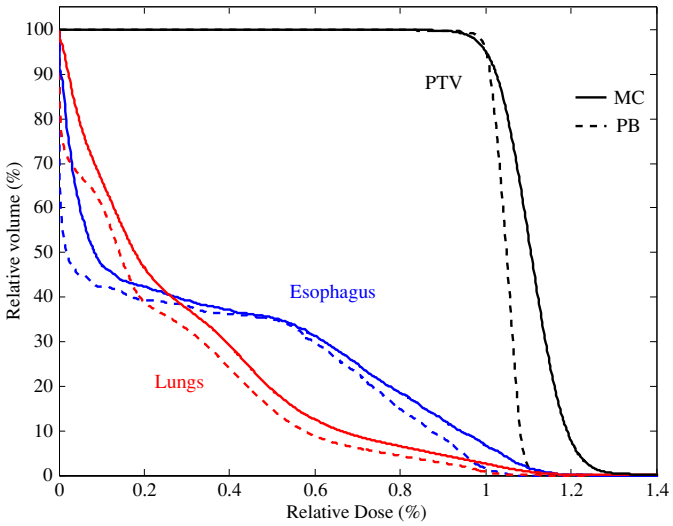

Figure 1. Dose–volume histogram: optimized IMRT plan based on Monte Carlo dose calculation (full lines) in comparison with pencil-beam-based dose calculation (dashed lines) normalized to 95% volume, corresponding to $D^{\text{pres}} = 63$ Gy.

4. Monte Carlo-based IMRT optimization

For this lung cancer patient, five beam directions were selected in the clinical treatment. We generate the corresponding five dose cubes for an open field using the MC simulations as described above. In the optimization, these dose cubes then serve as dose influence matrices, following equation (1). Because of high lateral scatters, these influence matrices are highly non-sparse and, thus, very memory intensive. However, a large portion of the matrix elements have vanishingly small values. Therefore, we utilize the method of voxel sampling (Martin *et al* 2007). This allows us to reduce the size of these dose influence matrices down to 1%, enabling us to perform an inverse planning optimization.

Figure 1 illustrates the dose–volume histogram (DVH) of this MC-based optimized plan (full lines). The dose is normalized to 95% of the PTV volume to receive the prescribed dose of 63 Gy, as discussed by Vanderstraeten *et al* (2006). Note that due to the large size of the lung tumor in this patient, it is not possible to apply a lower dose to the healthy portion of the lungs, while reaching the prescribed dose to the tumor. To contrast the outcome of an optimized plan which is based on PB dose calculation only, we plot the corresponding DVH in figure 1 as well (dashed lines). This comparison shows that an optimized IMRT plan based on PB dose calculation may appear to be a better plan in terms of PTV coverage, hot spots and OAR sparing. However, it deviates significantly from a Monte Carlo-based optimized plan that closely mimics the reality of the deposited dose. Figure 1 also illustrates that an otherwise optimal IMRT plan based on PB dose calculation may not correspond to the actual dose distribution because of these dosimetric errors. Therefore, errors in dose calculation cannot be neglected.

On the other hand, high-accuracy Monte Carlo dose calculations are computationally highly intensive and cannot be employed for practical. Therefore, we propose to sacrifice some precision for the sake of practicability. However, the impact of possible numerical errors to the final plan is yet another open question that can be addressed only in the retrospective,

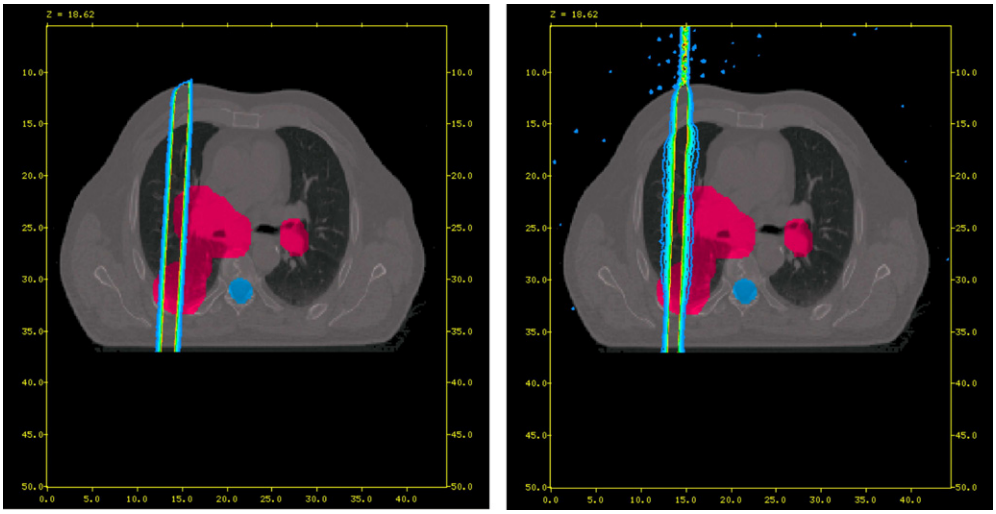

Figure 2. Two-dimensional representation of the deposited dose of one beamlet (1 cm^2): (left) using a pencil beam algorithm and (right) using Monte Carlo simulations. The circle shaped shaded region marks the spinal cord and all other shaded regions mark the PTV.

e.g. as errors to the DVH. In the following, we aim to address the issue of these dosimetric errors and how we can take them into account during the optimization process.

5. Dosimetric errors

The sources of dosimetric errors can depend on the underlying dose calculation algorithm, method of imaging and image processing, and other sources. Figure 2 shows that lateral dose distributions in lung are more accurately predicted by MC than PB because standard IMRT PB algorithms do not perform heterogeneity corrections in the lateral or transverse beam direction but only along the beam direction. Therefore, penumbra broadening is incorrectly predicted by PB algorithms and can lead to dose errors in the final dose plan if a large part of the PTV is composed of lung tissue.

To maintain the generality, we aim to employ an error model that is independent of the source. This approach restricts the use of more detailed knowledge about a particular source, i.e. we shall refrain from exploiting the difference between the more Gaussian lateral distribution of the MC dose and the sharp fall-off of the PB dose distribution.

In order to estimate the dosimetric errors, we choose a few significant beamlets and compute their dose distribution using both dose algorithms. Figure 2 illustrates this comparison for an example beamlet through the PTV. The MC-based beamlet reveals a significant lateral scattered dose. This lateral dose distribution is not captured with a PB-based beamlet at all. We conservatively estimate this difference to amount for an upper bound of 30% dosimetric error.

Since this work is intended as a proof of concept, we choose a 'worst-case' tumor scenario to capture most of possible scenarios. As shown in figure 2, the size and the location of the PTV in this patient clearly cover most cases of lung cancer, as observed in the past. Since the PTV half surrounds the spinal cord, we expect some cold spots in the final optimized plan to avoid overdose to OARs.

To model dosimetric errors, we randomly perturb the dose per monitor unit to each voxel of the PB-based dose influence matrix according to a normal distribution with zero mean and a

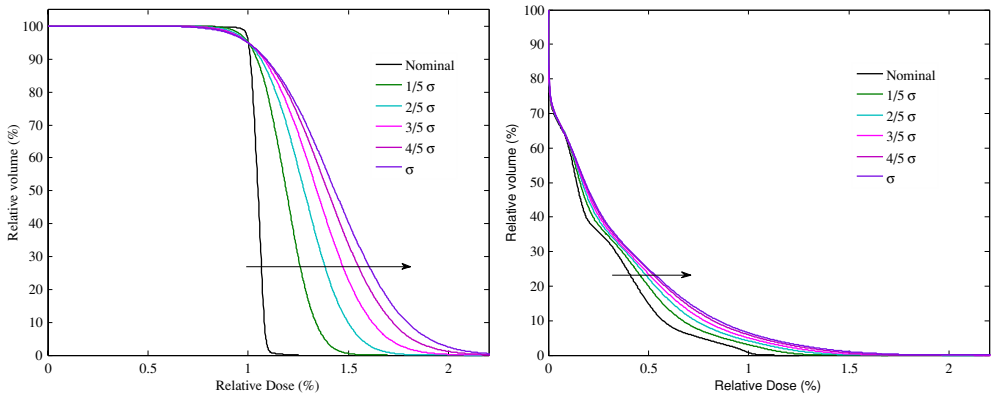

Figure 3. Dose–volume histogram for the PTV (left) and the combined lungs (right): five differently perturbed pencil-beam-based dose calculations are used to compute an optimized plan. The perturbation to the dose cube is to mimic the dosimetric uncertainties of the pencil-beam dose when compared to Monte Carlo-based dose calculations. The arrow indicates the order of the curves and dose values are normalized to 95% volume, corresponding to $D^{\text{pres}} = 63$ Gy.

standard deviation of $\sigma = 0.3$, which is motivated by the above conservative error estimation. To generate a larger set of perturbed dose cubes, we vary the size of the standard deviation as $\sigma/5$, $2\sigma/5$, $3\sigma/5$, $4\sigma/5$ and σ to obtain five different scenarios. Consequently, we compute optimized plans with respect to each of these PB dose cubes in order to evaluate the effects of dosimetric errors caused by insufficiently accurate dose models. Figure 3 illustrates that for larger dose errors, the deviation from the unperturbed plan is significant. In fact, for $\sigma = 0.3$, as is the case with respect to MC-based dose calculation, the PTV dose at 50% volume is increased by $\sim$35%.

While a PB-based dose calculation can be quite accurate for a homogeneous tissue density, it reveals larger deviations when larger heterogeneities are encountered, as is the case for lung cancer. Moreover, this deviation increases (to the first order linearly) with the magnitude of the perturbation. Therefore, a more accurate dose calculation warrants for a higher certainty and accuracy of the delivered plan.

6. Robust optimization model

As demonstrated in figure 3, an otherwise optimized IMRT plan can become suboptimal, when dosimetric, setup or other errors are encountered. In fact, this sub-optimality can become so significant that OARs might be exposed to unacceptable dose. Therefore, the issue of robustness is a first-order effect.

In the context of engineering design, there has been evidence illustrating that if errors are not taken into account during the decision process, the actual phenomenon can completely disappear (e.g. see Ben-Tal and Nemirovski (1998)). Recent works have been devoted to problems with convex objectives and constraints (e.g. linear). These works have shown that a convex optimization problem with parameter uncertainty can be transformed to another convex optimization problem. This transformation can be either exact or through a relaxation. However, the final problem can be more complex or can have a significantly larger number of constraints. The power of methods has been successfully tested on many applications, and we refer to Ben-Tal and Nemirovski (1998) and Bertsimas and Sim (2006). More recently,

local search methods have been expended to robust optimization of simulated-based problems. They entail finding descent directions and iteratively taking steps along these directions to optimize the robustness, i.e. reducing the worst-case cost. Interested readers should consult Bertsimas *et al* (2008) for a more in-depth introduction to these techniques.

While these works were devoted to managing the worst-case scenarios, combinatoric and stochastic optimization methods were employed to improve the statistically expected outcome, thus taking a more probabilistic approach, as has been applied to IMRT previously; see e.g. Bortfeld *et al* (2002) for sinusoidal motion.

We follow this probabilistic approach in the presence of dosimetric errors. In this study, the dose deposited to each voxel i is computed as

$$D_i(\mathbf{x}) = \sum_{j \in PB_i} d_{ij} \cdot \mathbf{x}_j, \tag{1}$$

where d_{ij} is the respective dose influence and $\mathbf{x}_j$ is a given fluence or beamlet intensity from the set of all beamlets PB. Following the discussion in section 5, we model the perturbed dose to each voxel d_{ij}^k as

$$d_{ij}^k = d_{ij} \cdot \left(1 + \delta_{ij}^k\right). \tag{2}$$

The independent random perturbation δ_{ij}^k follows a normal distribution $\mathcal{N}(0, \sigma_k)$. To capture errors of different magnitudes, we vary the size of σ^k to generate different dosimetric scenarios, as described in section 5. We can rewrite equation (1) for all error scenarios $k \in \mathcal{S}$ as

$$D_i^k(\mathbf{x}, \delta) = \sum_{j \in PB} d_{ij}\left(1 + \delta_{ij}^k\right) \cdot \mathbf{x}_j. \tag{3}$$

We denote the distribution of these dose scenarios D^k by $\mathcal{P}^k(\delta)$. Further knowledge of the nature of these errors can be exploited to adjust $\mathcal{P}^k(\delta)$. Otherwise, an equal or random weighting of the scenarios preserves the generality.

For the optimization, we employ a quadratic objective function, as also used by Unkelbach *et al* (2007), which is given by

$$E^k(\mathbf{x}, \delta) = \sum_{n \in \mathcal{V}} \frac{\alpha_n}{|V_n|} \sum_{i \in V_n} \left[D_i^k(\mathbf{x}, \delta) - D^{\text{pres}}\right]_+^2. \tag{4}$$

Note that $\mathcal{V}$ denotes the set of all voxels, divided in volumes of interest V_n with the corresponding weights α_n. These weights are chosen accordingly to satisfy the prescribed dose. In our lung cancer case, the prescribed dose to the PTV is $D^{\text{pres}} = 63$ Gy and to all critical structures it is $D^{\text{pres}} = 0$ Gy. The maximum dose to the spinal cord and esophagus is 45 Gy.

To determine a plan that is least sensitive to dosimetric errors, we formulate the robust optimization problem

$$\begin{aligned} &\min_x \langle E(\mathbf{x}) \rangle = \sum_{k \in \mathcal{S}} E^k(\mathbf{x}, \delta) \cdot \mathcal{P}^k(\delta) \\ &\text{subject to } x_i \geqslant 0 \end{aligned} \tag{5}$$

through a minimization of the expectation value of the deviations between the delivered and prescribed dose with uncertainty-model-based random perturbations. The robust optimization is conducted over five different beam angles, which correspond to a total number of more than 230 000 non-air voxels in the dose influence matrices for the unperturbed and each of the five perturbed scenarios. The search space of beamlet intensities encompasses 714 beamlets.

We implement this robust approach in a fashion that enables us to generate scenarios through a random variable that parametrizes the uncertainty model. Moreover, it yields the

dose to an anatomic voxel and its gradient with respect to the beamlet intensities. Thus, we can conduct a gradient-based optimization, which is highly efficient and does not require the detailed knowledge of the uncertainty. This capability allows for an extension to other sources of errors within the same framework.

7. Results

To measure the quality of the proposed robust algorithm, we conduct two different quantitative comparisons. First, we compare the beamlet intensities of the robust plans to the nominal scenario using PB dose influence matrices to compute the dose deposited. Next, we apply the same beamlet intensities (robust and nominal) to the MC dose influence matrix to probe their quality using this physically more reliable method.

7.1. Comparison with pencil-beam-based dose

Here, we compare the PB-based optimized beamlet intensities of the nominal scenario $\mathbf{x}^{\mathrm{PB,nom}}$ to the robust plans $\mathbf{x}^{\mathrm{PB,rob}}$. We use the unperturbed PB dose influence matrices $d_{ij}^{\mathrm{PB,unpert}}$ to compute the nominal and the robust dose deposited:

$$D_i^{\mathrm{PB,nom}} = \sum_{j \in PB} d_{ij}^{\mathrm{PB,unpert}} \cdot x_j^{\mathrm{PB,nom}}, \tag{6}$$

$$D_i^{\mathrm{PB,rob}} = \sum_{j \in PB} d_{ij}^{\mathrm{PB,unpert}} \cdot x_j^{\mathrm{PB,rob}}, \tag{7}$$

respectively. The DVH comparison between the nominal and robust solutions is shown in figure 4. For reference, the worst-case outcome is plotted as well which is computed via

$$D_i^{\mathrm{PB,worst}} = \sum_{j \in PB} d_{ij}^{\mathrm{PB},\sigma} \cdot x_j^{\mathrm{PB,nom}}. \tag{8}$$

Figure 4 demonstrates that the robust plan significantly outperforms the worst-case scenario. The comparison to the nominal solution shows the 'price of robustness' which means that in an error-free environment, the nominal solution clearly provides the better plan, in terms of both hot and cold spots in the PTV and healthy tissue sparing. However, we have demonstrated that the nominal case is not a realistic scenario. We also emphasize that the robust plan is optimized based on six differently perturbed $d_{ij}^{\mathrm{PB},\sigma_k}$ scenarios and clearly underperforms when applied to the non-perturbed $d_{ij}^{\mathrm{PB,unpert}}$.

7.2. Comparison with Monte Carlo-based dose

Assuming that MC dose calculation is the most realistic simulation of the physical dose deposition, we compare the nominal and robust solutions by using MC-based influence matrix d_{ij}^{MC} as follows:

$$D_i^{\mathrm{MC,nom}} = \sum_{j \in PB} d_{ij}^{\mathrm{MC}} \cdot x_j^{\mathrm{PB,nom}} \tag{9}$$

$$D_i^{\mathrm{MC,rob}} = \sum_{j \in PB} d_{ij}^{\mathrm{MC}} \cdot x_j^{\mathrm{PB,rob}}. \tag{10}$$

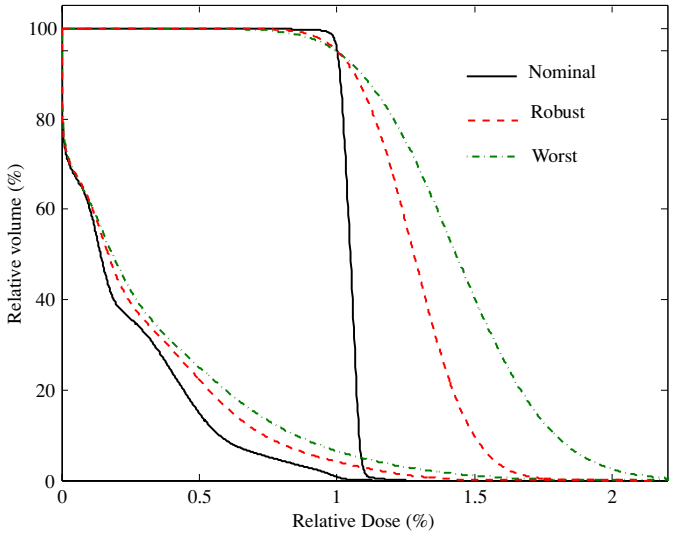

Figure 4. Dose–volume histogram: beamlet intensities optimized based on PB dose influence matrices are applied to three different PB dose influence matrices for a comparison among the nominal, robust and worst-case plans, according to equations (6)–(8), respectively. The dose is scaled to 95% volume, corresponding to D^{pres}.

The DVH of these two solutions in figure 5 illustrates how the nominal solution vastly fails to delivery any clinically relevant dose, since dosimetric errors introduced by the simplistic PB method are not taken into account. Figure 5 also demonstrates that when these errors are taken into account during the robust optimization, the plan is clinically relevant by avoiding hotspots in the PTV and delivering the prescribed dose to more than 90% of the PTV. As mentioned above, the large size and the position of the PTV in this particular patient cause some cold spots in the PTV; thus, the slope for $V \geqslant 90\%$.

As a reference, figure 5 also slows the optimized plan using MC influence matrices. While this plan is optimized based on a different dose calculation and, thus, not exactly comparable to the nominal and robust plans, we use it both as a guide for the eye and to qualify the robustly optimized plan as 'realistic' in terms of the physical dose deposited. We observe a dose distribution for the nominal plan which has a standard deviation about the prescribed dose that is 37.7% larger than the MC dose spread for the PTV. The dose distribution of the robust plan, however, exhibits only 18.7% deviation, which equates to a two-fold improvement.

An alternative comparison provides the concept of equivalent uniform dose (EUD) which probes the clinical relevance of dose distribution. The underlying assumption is that the uniform distribution of the corresponding biological equivalent dose will lead to the same cell-kill in the tumor as the actual non-uniform dose distribution. Following equation (1), we use the Niemierko (1999) concept of generalized EUD to compute

$$\text{EUD}_n = \left(\frac{1}{N_n} \sum_{i \in V_n} D_i^{a_n} \right)^{1/a_n} . \tag{11}$$

Since the PTV is the volume of interest V_n, we chose the exponent $a_n = -10$ to emphasize higher dose values. While we measure an EUD of 42.8 Gy for the nominal plan, the robust plan delivers an EUD of 53.6 Gy. Compared for an EUD of 64.0 Gy for the MC-based dose

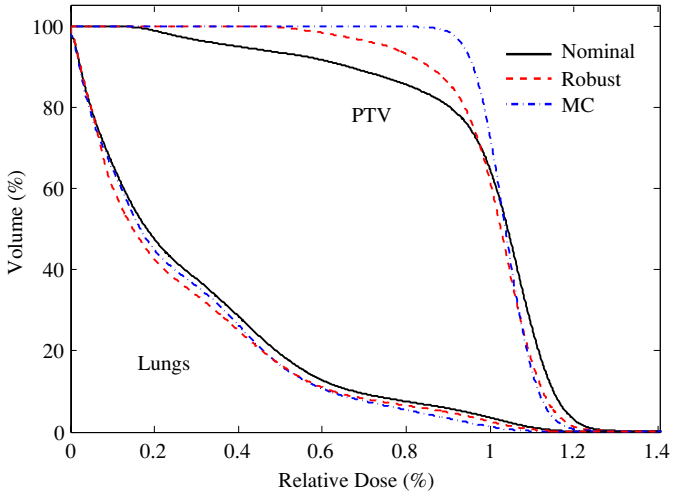

Figure 5. Dose–volume histogram: beamlet intensities optimized based on PB dose influence matrices are applied to MC-based dose influence matrices for a 'reality check' of physical dose deposited. The solid line corresponds to equation (9) and the dashed line to equation (10). The dashed-dotted line corresponds to a fully MC-based optimized plan, as shown in figure 1. All dose values are scaled to the prescribed 63 Gy dose to the PTV.

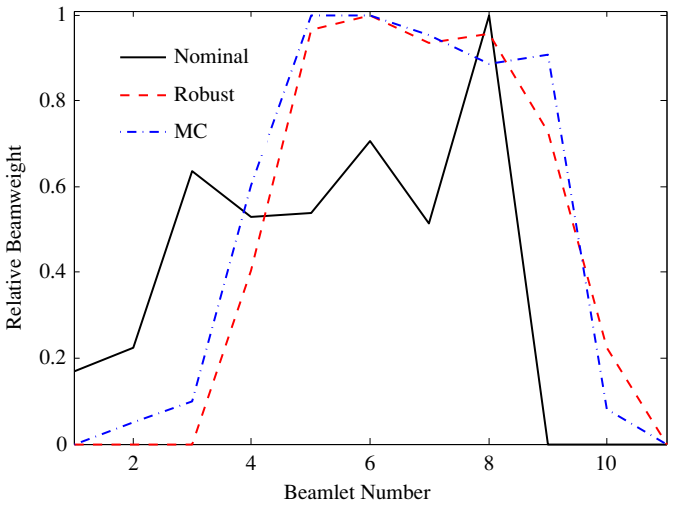

Figure 6. A comparison of the beamlet intensity profiles from the 325° direction as a cross section in the CT plain, as shown in figure 2. The field size from this direction is 15×11 cm^2. The nominal and robust plans are compared. The Monte Carlo-based plan is shown as a reference.

distribution, the nominal plan deviates by 33.1%, whereas the robust plan deviates by 16.3% exhibiting also a two-fold improvement.

We attribute the remaining difference to the MC spread to a few reasons. First, our model assumed randomly distributed errors for the sake of generality; thus, it did not intend to exactly mimic MC dose. Second, we do not take any numerical or imagining errors into account for the MC influence matrices and a MC worst-case scenario will certainly perform worse than the nominal shown here. Finally, the size and the location of the PTV of the discussed patient

impose unique challenges to the optimization, which are less pronounced in the MC dose calculation due to the less sharp lateral fall-off.

Nevertheless, both comparisons prove the concept of our algorithm, namely that when random perturbations are introduced to PB dose influence matrices, the presented robust optimization algorithm can provide plans that are not only significantly better than worst-case PB scenarios, but very well comparable to clinically relevant plans.

Since optimization solutions are often non-intuitive, for a better understanding of the difference between the nominal and robust solutions, we analyze the respective beamlet intensities. Figure 6 illustrates a comparison between representative beamlet intensity profiles of the nominal and the robust plans. We observe that the 'high-frequency' components (in the Fourier domain) of the nominal plan are smoothed out in the robust plan, since this solution takes into account more broadened lateral fall-off distribution than in the PB-based case. In addition, the smoother robust fluence profiles can be attributed to the fact that the robust problem in equation (5) is solved over a considerably larger search space as opposed to the nominal problem. These additional degrees of freedom warrant for a dose distribution, which closely resembles the actual physical dose delivered, as shown in the comparison to the MC profile. Since band-pass filters reduce the search space, we cannot assume that they would result in an inherently optimal robust solution as achieved with our proposed method.

8. Conclusion

In this paper, we introduced a robust optimization method to handle dosimetric errors in IMRT. Since these errors can significantly degrade treatment plans, our method provides plans that are robust against dosimetric errors. On the one hand, pencil-beam algorithms are very fast but inaccurate and, on the other hand, Monte Carlo algorithms are very accurate but computationally demanding. Therefore, this method relies on pencil-beam-based dose calculation and accounts for random perturbations in order to bring the final dose plan closer to the real delivered dose. In this study, this final robust plan is compared to Monte Carlo predictions to warrant clinical relevance. In our method, we used a generic error model and do not exploit any internal structure. Thus, this method is well suited to capture other sources of uncertainties as well.

We demonstrated the performance of this robust method on a lung cancer patient, as treated at the Massachusetts General Hospital. Due to the very large size and location of the tumor, this case was chosen for this proof of concept. We show that an otherwise optimal pencil-beam-based plan fails when its real dose deposit is measured. Using our method, however, we demonstrate that the robust plan performs well and matches in large parts the clinically relevant behavior. In fact, we observe a two-fold improved dose distribution and EUD for the robust plan when compared to the non-robust plan. Overall, this work demonstrates the potential of using our robust optimization methodology in IMRT planning to improve the quality of plans which encounter dosimetric errors. For the same accuracy, this method also offers a significant speedup when compared to Monte Carlo-based optimized plans. It also affords additional flexibility to the treatment planner to make suitable decisions regarding trade-offs based on a larger number of optimized plans in the same time.

Future work will include sequencing errors which can amount to 5%, imaging and contouring errors, numerical uncertainties and other sources of uncertainty that can degrade the final plan.

Acknowledgments

We would like to thank D Craft and G Sharp for fruitful discussions. We are also very grateful to H Paganetti for his insights as well as computation time. We would also like to thank N Choi for providing the lung patient data. This work was supported by the National Cancer Institute of the United States under grants R01-CA118200 and R01-CA103904. JS also acknowledges support from NIH grant R01 CA 111590.

References

Ben-Tal A and Nemirovski A 1998 Robust convex optimization *Math. Oper. Res.* **23** 769–805

Bertsimas D, Nohadani O and Teo K M 2009 Robust optimization for unconstrained simulation-based problems *Oper. Res.* at press (http://www.optimization-online.org/DB_HTML/2007/08/1756.html)

Bertsimas D and Sim M 2006 Tractable approximations to robust conic optimization problems *Math. Prog.* **107** 5–36

Bortfeld T, Jokivarsi K, Goitein M, Kung J and Jiang S B 2002 Effects of intra-fraction motion on IMRT dose delivery: statistical analysis and simulation *Phys. Med. Biol.* **47** 2203–20

Chan T, Bortfeld T and Tsitsiklis J N 2006 A robust approach to IMRT optimization *Phys. Med. Biol.* **51** 2567–83

Chu M, Zinchenko Y, Henderson S G and Sharpe M B 2005 Robust optimization for intensity modulated radiation therapy treatment planning under uncertainty *Phys. Med. Biol.* **50** 5463–77

Craft D and Bortfeld T 2008 How many plans are needed in an IMRT multi-objective plan database? *Phys. Med. Biol.* **53** 2785–96

Deasy J, Blanco A and Clark V 2003 CERR: a computational environment for radiotherapy research *Med. Phys.* **30** 979–85

Intensity Modulated Radiation Therapy Collaborative Working Group 2001 Intensity-modulated radiotherapy: current status and issues of interest *Int. J. Radiat. Oncol. Biol. Phys.* **51** 880–914

Jeraj R and Keall P 1999 Monte Carlo-based inverse treatment planning *Phys. Med. Biol.* **44** 1885–96

Küfer K H, Scherrer A, Monz M, Alonso F, Trinkaus H, Bortfeld T and Thieke C 2003 Intensity-modulated radiotherapy—a large scale multi-criteria programming problem *OR Spectr.* **25** 223–49

Martin B C, Bortfeld T R and Castanon D A 2007 Accelerating IMRT optimization by voxel sampling *Phys. Med. Biol.* **52** 7211–28

Niemierko A 1999 A generalized concept of equivalent uniform dose *Med. Phys.* **26** 1100

Seco J, Sharp G, Turcotte J, Gierga D, Bortfeld T and Paganetti H 2007 Effects of organ motion on IMRT treatments with segments of few monitor units *Med. Phys.* **34** 923–34

Seco J, Sharp G, Wu Z, Gierga D, Buettner F and Paganetti H 2008 Dosimetric impact of motion in free-breathing and gated lung radiotherapy: a 4D Monte Carlo study of intrafraction and interfraction effects *Med. Phys.* **35** 356–66

Sempau J, Wilderman S J and Bielajew A F 2000 DPM, a fast, accurate Monte Carlo code optimized for photon and electron radiotherapy treatment planning dose calculations *Phys. Med. Biol.* **45** 2263–91

Siebers J, Kawrakow I and Ramakrishnan V 2007 Performance of a hybrid MC dose algorithm for IMRT optimization dose evaluation *Med. Phys.* **34** 2853–63

Unkelbach J, Chan T C Y and Bortfeld T 2007 Accounting for range uncertainties in the optimization of intensity modulated proton therapy *Phys. Med. Biol.* **52** 2755–73

Vanderstraeten B, Duthow W, Gersem W D, de Neve W and Thierens H 2006 Fluoro-deoxy-glucose positron emission tomography voxel intensity-based intensity-modulated radiation therapy (IMRT) for head and neck cancer *Radiother. Oncol.* **79** 249–58

Zakarian C and Deasy J O 2004 Beamlet dose distribution compression and reconstruction using wavelets for intensity modulated treatment planning *Med. Phys.* **31** 368–75